ELECTROLUMINESCENCE IMAGING OF PV DEVICES: UNCERTAINTY DUE TO OPTICAL AND PERSPECTIVE DISTORTION

K.G. Bedrich*, M. Bliss, T.R. Betts, R. Gottschalg
Centre for Renewable Energy Systems Technology (CREST), School of Electronic, Electrical and Systems Engineering, Loughborough University, Loughborough, Leicestershire, LE11 3TU, UK
*Corresponding Author Tel.: +44 1509 635 355, Email: K.Bedrich@lboro.ac.uk

ABSTRACT: Electroluminescence (EL) images taken from on-field measurements often suffer from optical and perspective distortion affecting the interpretation and quantification of the images taken. Methods to correct these distortions are presented as well as a method to assess the associated uncertainties. This method uses the uncertainty of pixel position as intermediate step. The influence of pixel deflection, re-projection error and depth-of-field blur is evaluated. Three different camera systems are compared regarding tilt angle dependence. The re-projection error and the camera's focal length are identified as major influence on the resulting uncertainty. It was shown that EL images with sufficient quality can be recovered, from images taken at high perspective misalignments with tilt angles of about 50°.

Keywords: Electroluminescence, Devices, Calibration, Uncertainty, Evaluation

1 INTRODUCTION

Electroluminescence (EL) imaging is a fast and relatively simple method for the spatial analysis of PV devices. It was first proposed by Fuyuki et al. [1]. The basic setup consists of a near-infrared-sensitive camera and a power supply. It is mobile and therefore allows measurements not only in laboratories and factories, but also for quality control of installed systems in the field.

However, on-site measurements typically have limited angles and distances between camera and PV device which can result in perspective distortion, which in turns affects the interpretation of data. Low cost or wide angle optics will additionally increase lens (respective 'barrel') distortion. Little attention has been given to the removal of these artefacts nor has the associated uncertainty been investigated, despite this information being used to potentially verify warranty cases. This would be essential when moving from manual qualitative analysis to an automated and quantitative inspection as necessary for efficient early fault detection of PV devices.

This work quantifies uncertainty, expressed as standard deviation of the pixel position. From this the intensity uncertainty can be calculated. Due to the nature of the data being represented as 2D images, this uncertainty is given in the same format. A brief explanation of methods used for lens and perspective correction will be given and the dominating uncertainties will be identified. The resulting uncertainty maps will be applied to EL images of a PV module taken by different setups. Eventually the influence of different camera systems and the modules tilt angle will be compared.

2 CAMERA LENS DISTORTION

The shape of the used camera lens and positioning errors during the assembly of the camera can result in radial and tangential distortion of the EL image. A camera calibration, based for example on a chessboard pattern, photographs the calibration patterns in different positions and angles (Figure 1). Usually, the position of the features in the calibration pattern of 20 or more images are evaluated to calculate the lens distortion coefficients and the camera's intrinsic matrix C (defined by focal length and optical centre). An overview of this established method is given in [2–4]. The effect of camera lens distortion is demonstrated in Figure 2. It is clearly visible that the radial distortion on the left is manly removable. Distorted angles and positions can be recovered. OpenCV, an open source C++ framework for computer vision, implements various routines for this calibration [2].

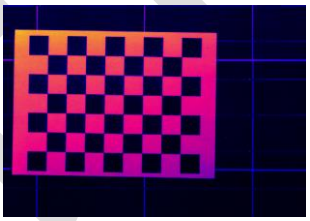

Figure 1: Image (1/20) used for camera calibration based on OpenCV

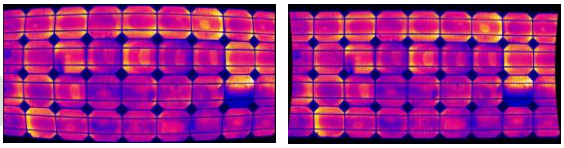

Figure 2: EL image of a PV module before (left) and after removal of lens distortion (right). Distortion exaggerated for clarification

3 PERSPECTIVE DISTORTION

For on-site measurements it is often not possible to keep a normal angle between PV device and optical axis, which results in perspective distortion. Skewed angles and different EL signal intensities are the consequence. Figure 3 shows a perspective correction which can be realized by applying the following steps:

1. Estimate the translation and shear matrix of the PV device. This can be done by either using the four corner points as well as the aspect ratio of the device or by comparing the EL image with a template EL image, free from perspective distortion (e.g. using pattern recognition).
2. Estimate the orientation of the PV device, using the four corner points.
3. With these angles and the camera's focal length, calculate and divide the image by the tilt factor, derived from the Kang-Weiss vignetting function [5].

4. Apply a perspective transformation on the intensity-corrected image using the matrix obtained in 1.

Estimation of rotation and translation, pattern recognition and perspective transformation can be done using OpenCV. Further explanation is given in [3, 6, 7].

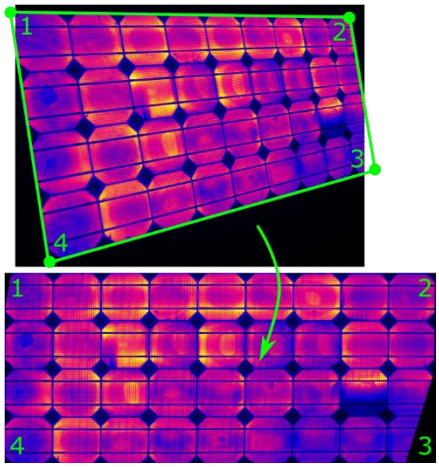

Figure 3: Scheme of perspective transformation of a module with the tilt angles $\alpha_x = 15°, \alpha_y = 30°$

4 UNCERTAINTY ANALYSIS

The following sections focus on uncertainty due to lens and perspective distortion. Other uncertainty contributors, like signal smearing, noise and vignetting issues are excluded and will be addressed in another publication. The uncertainty will be first described by multiple parameters $\overrightarrow{u_i}$ influencing the standard deviation of the position (x, y) of each image pixel. At the end of this section the combined position uncertainty $\overrightarrow{u_{pos}}$ will be translated to the actual pixel-intensity based uncertainty σ_{int}.

In this work all individual uncertainties are treated as independent and uncorrelated with a sensitivity of one. Consequently the combined position uncertainty becomes:

$$\overrightarrow{\sigma_{pos}} = \sqrt{\sum \overrightarrow{u_i}^2} \tag{1}$$

4.1 Lens and perspective deflection $\overrightarrow{\sigma_{lens}}$ and $\overrightarrow{\sigma_{persp}}$

The correction of both lens and perspective distortion can cause image areas to shrink and expand. Intermediate pixels will be used to interpolate between diverted pixels, increasing the deflection uncertainty. Figure 4 gives a simplified example using only the x dimension. There, the green area indicates an area to be expanded due to deflection. Its size doubles during the remap (a-b). Likewise the pixel indices map $m_{x,y}$ changes.

The increase of pixel size can be expressed from its inverse gradient as:

$$\overrightarrow{f_{px}} = \begin{pmatrix} \left|\frac{dx}{dm_x}\right| \\ \left|\frac{dy}{dm_y}\right| \end{pmatrix} \tag{2}$$

This factor measures the expansion of the original pixel size. Its average is equal to the area ratio of new to old device given in equation (8).

All position uncertainties based on the distorted image (here: $\overrightarrow{\sigma_{lens}}$) have to be multiplied with $\overrightarrow{f_{px}}$ to apapt to the pixe size of the corrected image.

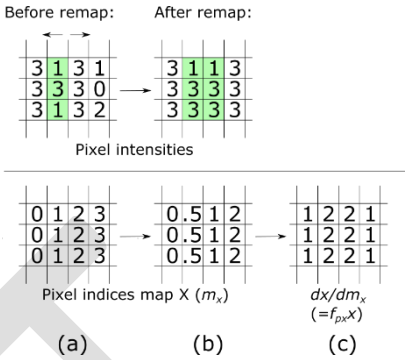

Figure 4: Scheme of deflection uncertainty of the x-axis due to image remapping

The uncertainty due to the interpolation between known pixels is assumed to be uniform or rectangular distributed. The corresponding standard distribution for both lens and perspective deflection (# as placeholder) can be obtained as follows [8]:

$$\overrightarrow{\sigma_{\#}} = \frac{\overrightarrow{f_{px-\#}} - 1}{2 \cdot \sqrt{3}} \tag{3}$$

4.2 Re-projection error σ_{rep}

This error originates from the root-mean-square of the difference between detected features within the camera calibration pattern and re-projected points [7]. Thus, this error estimates directly the uncertainty of a pixel position after correction from lens distortion. In this work the individual differences where indifferent from the image position. Therefore the uncertainty due to the re-projection error is assumed to be spatially uniform.

Because this parameter is based on the uncorrected image it has to be scaled by the area ratio in (8) to adapt to the size of the corrected image.

4.3 Depth of field blur σ_{DOF}

If the angle between optical axis and image plane is not perpendicular, certain areas of the PV device will be out of focus. The depth of field (DOF) sensitivity is mainly dependent on the camera lens' f-number and focal length. Pertuz et al. [9] described this defocus σ_{DOF} as a function of the distance d between lens and image plane as:

$$\sigma_{DOF} = \frac{k}{A} \cdot \frac{f^2 \cdot |d - d_f|}{d \cdot (d_f - f)} \tag{4}$$

Here A is the f-number of the camera lens, f the focal length, d_f the in-focus distance and k is a camera dependent parameter relating the blur circle to an actual point spread function (PSF). In this work the PSF (blur function) is assumed to be Gaussian distributed and therefore k is set to 2.335 as ratio of the full width at half maximum (FWHM) over standard distribution.

A depth map of the image plane $d(x,y)$ could be measured with a depth sensitive camera but can also be estimated from the four corner points of the PV device. OpenCV provides the function cv::solvePnP which returns a translation vector t and rotation vector r. Together with cv::Rodrigues (which transforms r to a rotation matrix R) and the camera position $\vec{c} = R^T \cdot \vec{t}$ the depth map $d(x,y)$ can be calculated as follows:

$$d(x,y) = R^{-1} \cdot \left(s \cdot (C^{-1} \cdot \begin{bmatrix} x \\ y \\ 1 \end{bmatrix}) \right) - t) \qquad (5)$$

With $s = \frac{(R^{-1} \cdot t)[2]}{\left(R^{-1} \cdot C^{-1} \cdot \begin{bmatrix} x \\ y \\ 1 \end{bmatrix}\right)[2]}$ and C being the camera matrix [7].

4.4 Neglected uncertainty factors

a) Object corner position

The uncertainty of the position of the four PV device's corners, needed for perspective correction, will depend on the method to identify them (manual or automated via pattern or object recognition). For this work the PV device corners in Figure 3 were defined by hand and the position error is assumed to be near zero. Therefore this factor was neglected.

If included, the corner position uncertainty will result in an additional position uncertainty map built through interpolation between the given four corner uncertainties as described in [10] and an additional intensity uncertainty map due to different tilt factors. The tilt factor is calculated from the rotation angles of the image plane and modifies the vignetting effect.

b) Interpolation error

The non-integer values within the pixel index map $m_{x,y}$ result in data interpolation using the neighbouring pixels. The interpolation methods can be distinguished by the number and weights of the neighbours. Every method (nearest neighbour, bi-linear, cubic etc.) will be a trade-off between introduced blur and precision. The uncertainty induced by interpolation is thought to low as it is not a dominating factor in the overall uncertainty.

4.5 Intensity uncertainty σ_{int}

So far the uncertainty is given as standard deviation σ_x , σ_y of all pixels in x and y dimension, indicating their blurriness. To transform these values into uncertainty of pixel intensities the following steps are conducted on every image pixel:

1. Calculate a local point spread function $PSF_{x,y}$ as Gaussian distribution $f(\sigma_x, \sigma_y)$.
2. Multiply the difference to all neighbour pixels within the PSF (size=2s+1) with the respective PSF value.
3. The sum of all differences gives the local intensity uncertainty:

$$\sigma_{int}[x,y] = \sum_{i=-s}^{s+1} \sum_{j=-s}^{s+1} |I[x,y] - I[x+i, y+j]| \cdot PSF_{x,y}[i,j] \qquad (6)$$

The resulting map σ_{int} will be sensible to high gradient variations. This is perspicuous, because blur does not affect low gradient changes, as to be found in e.g. the image background but high gradient changes e.g. cell borders or busbars.

5 PV MODULE UNCERTAINTY MAPS

The uncertainty maps of the different distortions are shown in Table 1. It shows the combined position uncertainty, their individual contributors and the pixel intensity uncertainty for the corrected EL image in Figure 3 (bottom). Regarding the scale of the individual uncertainty contributors it is clear that $\overrightarrow{\sigma_{pos}}$ is dominated by perspective deflection which is in turn defined by rotation in α_y. Up to one and two decades lower is the influence of DOF blur and lens deflection. It can be neglected for the used camera system.

The intensity uncertainty σ_{int} is related to the EL image itself to show the relative uncertainty. It can be seen that σ_{int} is highest at the left and right image border due to the likewise higher $\overrightarrow{\sigma_{pos}}$ values. The σ_{int} map reminds of a gradient image. This is indeed plausible because even a high uncertainty of pixel positions wouldn't influence the image in homogenous areas. At cell borders or busbars however, even a small position uncertainty of one pixel would vary whether the image intensity is low (background) or high (EL signal).

Table 1: Resulting uncertainty maps for Figure 3 (bottom)

Lens deflection $|\overrightarrow{\sigma_{lens}}|$

Depth-of-field blur $|\overrightarrow{\sigma_{DOF}}|$

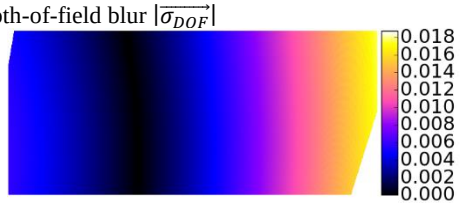

Perspective deflection $|\overrightarrow{\sigma_{persp}}|$

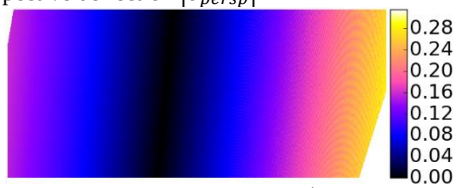

Combined position uncertainty $|\overrightarrow{\sigma_{Pos}}|$

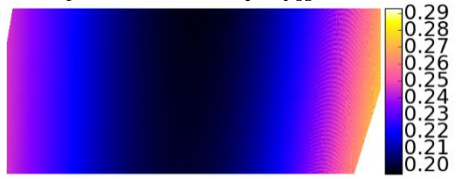

Relative intensity uncertainty $100 \cdot \frac{\sigma_{int}}{I}$

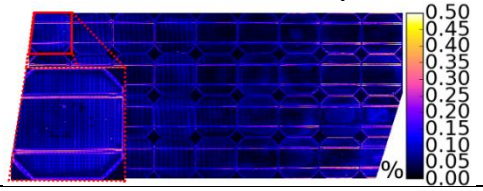

In contrast to this, Table 2 shows the resulting uncertainty maps for an EL image, artificially distorted with a higher tilt angle. The increased tilt angle clearly increased all contributors to perspective distortion, resulting in a three times higher position uncertainty and an intensity uncertainty over 3% at busbars.

Table 2: Resulting uncertainty maps for an artificially distorted EL image

EL image at title angle $\alpha_x = \alpha_y = 51°$

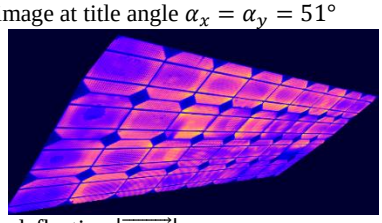

Lens deflection $|\overrightarrow{\sigma_{lens}}|$

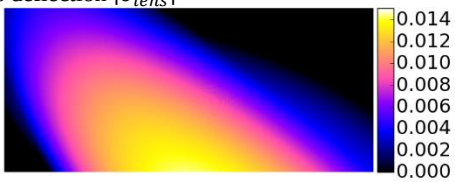

Depth-of-field blur $|\overrightarrow{\sigma_{DOF}}|$

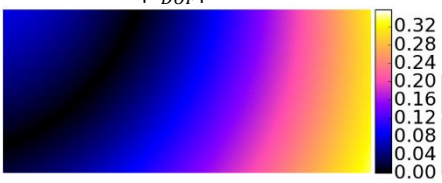

Perspective deflection $|\overrightarrow{\sigma_{persp}}|$

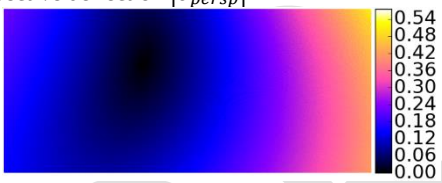

Combined position uncertainty $|\overrightarrow{\sigma_{Pos}}|$

Relative intensity uncertainty $100 \cdot \frac{\sigma_{int}}{I}$

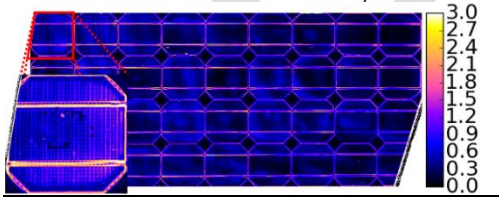

6 INFLUENCE OF CAMERA SYSTEM AND PERSPECTIVE

To compare the influence due to different optics, camera calibrations of three very different cameras where used:

a) SensoCam 830HR: CCD used for EL imaging
b) Logitech C210: consumer product webcam
c) Nexus 5: Mobile phone camera with built-in optics

All cameras have different resolutions, focal lengths and DOF ranges. This difference becomes visible when comparing the averaged position uncertainty values for EL images corrected from different tilt angles (α_x, α_y) as shown in Table 3. Here, heat maps were created from 400 different tilt angles between 0 and 65°.

To establish perspective distortion, the four module corners in the undistorted EL image (Figure 3, bottom) where rotated in 3D and projected back accordingly. The resulting quadrilateral was scaled to use the maximum available image space. The position uncertainty was calculated as described in Section 4. This parameter estimates the standard deviation of the pixel position in the corrected image and dependents on the size of which. The averaged results might be therefore misleading because the high α_y values will stretch the original image resulting in likewise high deflection uncertainties. A more comparable parameter can be obtained, if $|\overrightarrow{\sigma_{pos}}|$ is scaled with the ratio of image pixels before and after correction as follows:

$$|\overrightarrow{\sigma_{pos-rel}}| = \frac{|\overrightarrow{\sigma_{pos}}|}{r_A} \tag{7}$$

$$r_A = \frac{sizeX_{corr} \cdot sizeY_{corr}}{A_{dist}} \tag{8}$$

$$A_{dist} = 0.5 \cdot |(c3x - c1x) \cdot (c4y - c2y) + (c4x - c2x) \cdot (c1y - c3y)| \tag{9}$$

A_{dist} is the area of an irregular quadrilateral built by the four corners c1-c4. $|\overrightarrow{\sigma_{pos-rel}}|$ can be interpreted as average position uncertainty of a pixel within the distorted image.

Table 3: Angle dependency of absolute and relative position uncertainty [px] for three different camera systems

Type	$\lvert\overrightarrow{u_{pos}}\rvert$	$\lvert\overrightarrow{u_{pos-rel}}\rvert$
a	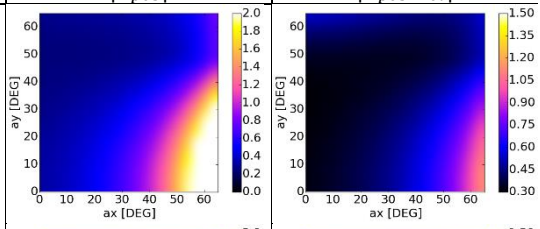	
b	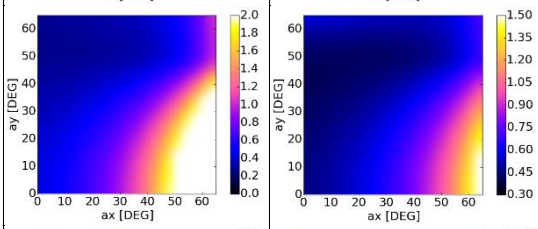	
c	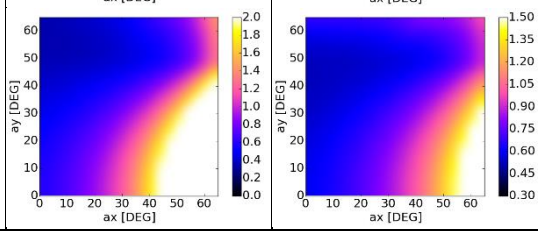	

The heat maps in Table 3 allow the following conclusions:

$|\overrightarrow{\sigma_{pos}}|$ increases slightly from camera type (a) to (c), respective values at $\alpha_x = \alpha_y = 45°$ increase from 0.5 to 0.7.

High α_x angles result in higher position uncertainties than angles in α_y, which is due to the fact that increasing α_y angles decrease the visible aspect ratio of the PV module and allow a better fit within the image. An area of distinctively smaller uncertainty can therefore be found for high α_y and moderate α_x especially for type (a). Here, the additional tilt α_x not only improved the aspect ratio but also unskewed the distorted EL image to a certain extent.

This allows the assumption that even high tilt angles don't necessarily make corrected images unusable for quantitative analysis. However, in practice highly distorted images will also have high interpolation errors as discussed in Section 4.4.

Figure 5 compares the individual influence of all regarded uncertainties to $\overrightarrow{\sigma_{pos}}$ for increasing tilt angles. It can be seen that the re-projection error σ_{rep} from lens distortion removal dominates the other uncertainty sources. Although σ_{rep} doesn't have an angle dependency it is scaled with the area ratio r_A to adapt to the new pixel size. It can be seen that σ_{rep} increases from camera type (a) to (c). This can be due to an insufficient camera calibration or optical distortions that couldn't be fitted adequate by the lens distortion model, given in [2].

The perspective deflection uncertainty however doesn't vary for the different camera types due to the fact that perspective correction only depends on the four given object corners. In contrast to this the DOF uncertainty is highly dependent on the used optics. As demonstrated in (4), the camera's focal length has a squared influence on σ_{DOF}. This can dominate for high tilt angles or long focal lengths. Lens deflection, however, can be neglected for these cameras. This might change if a wide angle (fish eye) lens is used.

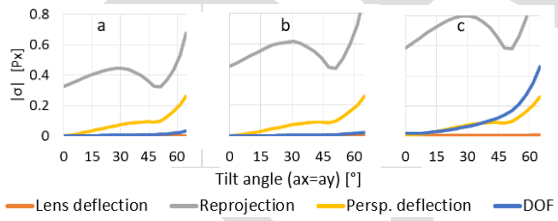

Figure 5: Influence of individual uncertainties at different tilt angles

7 SUMMARY AND CONCLUSION

This paper presents a method to correct from perspective and lens distortion and to measure the pixel intensity uncertainty using the uncertainty of pixel position as intermediate step. Exemplary uncertainty maps derived from the correction of a PV module are shown and discussed as well as the influence of tilt angle and camera type. Re-projection error and focal length are identified as major influence to the combined position uncertainty σ_{pos}.

The absolute position uncertainty being under 2 pixel for most tilt angles shows that images with perspective and optical distortion can still be used for quantitative analysis. However the inhomogeneity within the position uncertainty increases with increasing tilt. PV device corners especial at the opposed side of the camera can be treated as insufficient due to high distortion.

However, measures and thresholds limiting the quality of EL images don't currently exist. Defining a minimum object resolution, given by pixel resolution and localized point spread function, as well as a compulsory representation of EL images free from distortion and camera effects would be beneficial for quantitative analysis. With $\overrightarrow{\sigma_{pos}}$ and σ_{Int} as localized position and intensity uncertainty, this paper provides a simple measure to qualify the impact on EL images and clearly highlights the differences when using low quality optics and inappropriately strong perspective. This allows EL images taken on field to be corrected and evaluated almost equally to images taken in lab conditions.

It is aimed to release the code for calculating position and intensity uncertainty within an interactive graphical environment in the near future.

REFERENCES

[1] T. Fuyuki, H. Kondo, T. Yamazaki, Y. Takahashi, and Y. Uraoka, "Photographic surveying of minority carrier diffusion length in polycrystalline silicon solar cells by electroluminescence," *Appl. Phys. Lett.*, vol. 86, no. 26, p. 262108, 2005.

[2] V. Pisarevsky, "Introduction to OpenCV," *Agenda*, vol. 42, pp. 433–434, 2010.

[3] M. Fiala and C. Shu, "Self-identifying patterns for plane-based camera calibration," *Mach. Vis. Appl.*, vol. 19, no. 4, pp. 209–216, 2008.

[4] A. Datta, J.-S. Kim, and T. Kanade, "Accurate camera calibration using iterative refinement of control points," *2009 IEEE 12th Int. Conf. Comput. Vis. Work. ICCV Work.*, pp. 1201–1208, Sep. 2009.

[5] S. Lin, "Single-Image Vignetting Correction," *2006 IEEE Comput. Soc. Conf. Comput. Vis. Pattern Recognit. - Vol. 1*, vol. 1, pp. 461–468, 2006.

[6] G. K. a and M. S, "Automatic Rectification of Perspective Distortion from a Single Image Using Plane Homography," *Int. J. Comput. Sci. Appl.*, vol. 3, no. 5, pp. 47–58, Oct. 2013.

[7] G. Bradski and A. Kaehler, *Learning OpenCV: Computer vision with the OpenCV library*. O'Reilly, 2008.

[8] I. BIPM, I. IFCC, I. IUPAC, and O. ISO, *Evaluation of measurement data—guide for the expression of uncertainty in measurement. JCGM 100: 2008*, no. September. 2008.

[9] S. Pertuz, D. Puig, and M. A. Garcia, "Analysis of focus measure operators for shape-from-focus," *Pattern Recognit.*, vol. 46, no. 5, pp. 1415–1432, May 2013.

[10] S. Schlegel, N. Korn, and G. Scheuermann, "On the interpolation of data with normally distributed uncertainty for visualization," *IEEE Trans. Vis. Comput. Graph.*, vol. 18, no. 12, pp. 2305–2314, 2012.